Spectroscopy on the B850 Band of Individual Light-Harvesting 2 Complexes of *Rhodopseudomonas acidophila* II. Exciton States of an Elliptically Deformed Ring Aggregate

M. Matsushita,* M. Ketelaars,† A. M. van Oijen,* J. Köhler,‡ T. J. Aartsma,† and J. Schmidt*
*Centre for the Study of Excited States of Molecules, Huygens Laboratory, and †Department of Biophysics, Leiden University, 2300 RA Leiden, The Netherlands; and ‡Experimental Physics IV, University of Bayreuth, 95440 Bayreuth, Germany

ABSTRACT Spectroscopy of individual light-harvesting 2 complexes from purple photosynthetic bacteria revealed a deformation of the circular complex into C_2 symmetry. The present work relates the geometry of the deformed aggregate to its spectroscopic properties. Different models of elliptical deformation are discussed and compared with the experimental findings. It is shown that the model with smaller interpigment distances, where the curvature of the ellipse is small, provides the best agreement with fluorescence excitation spectra of individual complexes.

INTRODUCTION

Study of the photo-excited states of light-harvesting pigment-protein complexes is the first step towards a quantitative understanding of the initial processes of photosynthesis, in which light energy absorbed by pigments is transferred efficiently to the photochemical reaction center. The geometrical arrangement of the pigments in the complexes plays an essential role in the delocalization of the excitation over a number of pigments and in the mechanism of energy transfer among them. When a complex has a high geometrical symmetry and the coupling between the pigments is large, the excitation of equivalent pigments may be delocalized. An example is the B850 ring of the light-harvesting 2 (LH2) complex of the photosynthetic purple bacterium *Rhodopseudomonas acidophila*. From the x-ray crystal structure the complex is known to have C_9 symmetry (McDermott et al., 1995). The B850 ring consists of 18 bacteriochlorophyll (BChl) *a* molecules, which are arranged in a circle with the inter-pigment distance <10 Å. The absorption of the B850 ring around 850 nm originates from the Q_y transitions of the BChl *a* molecules. The interaction between the Q_y transition dipoles of adjacent BChl *a* molecules was estimated to be $200 \sim 400$ cm^{-1} (Sauer et al., 1996; Alden et al., 1997; Koolhaas et al., 1998, 2000; Krueger et al., 1998; Sundström et al., 1999; Scholes et al., 1999; Scholes and Fleming, 2000) which gives rise to the exciton band width of around 1000 cm^{-1}. It is expected that perfect delocalization of the excitation is not achieved, since the local protein environment is not identical for all the pigments. It is difficult to evaluate the random energetic disorder within the B850 ring, because the heterogeneity among different complexes adds extra broadening in usual ensemble measurements. Lack of the exact value of both the interaction strength and the random disorder prevents a precise characterization of the electronic excitations in the B850 band.

Recent spectroscopic studies of individual LH2 complexes provide unprecedentedly detailed information usually hidden by ensemble averaging (Bopp et al., 1997; van Oijen et al., 1998, 1999a, b, 2000; Tietz et al., 1999; Bopp et al., 1999; Ketelaars et al., 2001). The observation of the exciton states of a single complex enables a precise determination of the interaction strength (Ketelaars et al., 2001), whereas information about disorder can be obtained from the statistics of the spectra from several individual complexes (van Oijen et al., 2000). In addition to the random disorder, the observed spectra indicated the presence of a regular modulation of the interaction between the different pigments (van Oijen et al., 1999b; Bopp et al., 1999). The present work focuses on the physical origin of this modulation.

In the accompanying paper (Ketelaars et al., 2001) a detailed account is given of the spectroscopic observations carried out on individual LH2 complexes and which confirm the earlier conclusion (van Oijen et al., 1999b) that a modulation of C_2 symmetry exists in the interpigment interaction. This result indicates that the isolated complex in the host matrix is deformed in a well-defined manner from the perfect C_9 symmetry observed in the x-ray crystal structure analysis. A room temperature study of the fluorescence from individual complexes led to a similar conclusion that the complex behaves like an elliptical absorber (Bopp et al., 1999). The aim of the present work is to provide a link between the geometrical deformation and the spectroscopic properties of the individual LH2 complex.

A circular aggregate and C_2 perturbation

This section describes the exciton states of the B850 ring subjected to a C_2 perturbation. The LH2 is a nanomeric cyclic aggregate of $\alpha\beta$ polypeptide heterodimers. Reflect-

Received for publication 28 August 2000 and in final form 19 December 2000.

Address reprint requests to Dr. Michio Matsushita, Leiden University, Centre for the Study of Excited States of Molecules, Huygens Laboratory, P. O. Box 9504, 2300 RA, Leiden, The Netherlands. Tel.: 31-71-527-5909; Fax: 31-71-527-5819; E-mail: michio@molphys.leidenuniv.nl.

0006-3495/01/03/1604/11 $2.00

ing the nanomeric structure of LH2, the B850 ring has C_9 symmetry and consists of nine repeating pairs of α- and β-bound BChl *a* molecules. The ring of the 18 Q_y transition moments slightly deviates from C_{18} symmetry due to the different orientations of the α- and β-bound molecules. In addition, the different local environments of the binding sites make the excitation energy different for the α- and β-bound molecules. The different excitation energy has been pointed out to be important for the circular dichroism, whereas it has little influence on the absorption spectrum (Koolhaas et al., 1997). The purpose of the present work is to discuss and compare different models for an elliptical deformation of the B850 ring. To make the comparison easier, we will take the simplest description of the unperturbed circular ring with the minimum number of free parameters by neglecting the difference between the α- and β-bound molecules and assuming C_{18} symmetry. The C_{18} assumption is justified by the following arguments. First, the absorption spectrum is not sensitive to the difference between the excitation energies of the α- and β-bound molecules, and second, the orientational difference between those molecules is much smaller than the deformation we will discuss. The correspondence between the properties of the B850 ring in C_9 symmetry and the C_{18} approximation is given in Appendix A. We also neglect the transition moment along the symmetry axis, which carries less than 2% of the total absorption intensity. The B850 ring in C_{18} symmetry is shown in Fig. 1. The orientation of the Q_y transition dipole moment corresponds to the average orientation of those of the α- and β-bound molecules. This yields a tilt of 24.5 degrees of the Q_y transition dipole from the local tangent. From experiments on individual complexes the average nearest-neighbor interaction was determined to be $V_0 = -240\ \mathrm{cm}^{-1}$ (Ketelaars et al., 2001).

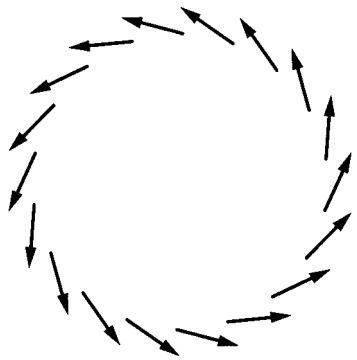

FIGURE 1 Position and orientation of the 18 Q_y transition dipole moments of the unperturbed B850 ring. In order to obtain C_{18} symmetry, the position and orientation of the α- and β-bound BChl *a* molecules have been averaged. The transition moment along the symmetry axis is neglected.

The Hamiltonian describing a singly excited Frenkel exciton of the unperturbed C_N ring is given by

$$H_0 = E_0 \sum_{n=1}^{N} |n\rangle\langle n| + V_0 \sum_{n=1}^{N} [|n\rangle\langle n+1| + H.c.]$$

$$+ W_0 \sum_{n=1}^{N} [|n\rangle\langle n+2| + H.c.], \quad (1)$$

where E_0 is the Q_y transition energy, and V_0 and W_0 are the nearest- and the second-neighbor interactions, respectively. In the present work the inter-pigment interactions are taken into account up to the second neighbors. The eigenfunction and the energy of the exciton states are given by

$$|k\rangle = \frac{1}{\sqrt{N}} \sum_{n=1}^{N} \exp(ik\phi n)|n\rangle, \quad (2)$$

$$E_k = E_0 + 2V_0\cos(k\phi) + 2W_0\cos(2k\phi), \quad (3)$$

where $\phi = 2\pi/N$ and $k = 0, \pm 1, \pm 2, \ldots, \pm(N/2 - 1), N/2$. In the unperturbed ring of $N = 18$, the exciton states are doubly degenerate except for the lowest, $k = 0$, and highest, $k = 9$, states. The oscillator strength in the plane of the ring is exclusively concentrated in the $k = \pm 1$ states. Because of the circular symmetry, the transitions to the degenerate $k = \pm 1$ states can be decomposed into two linearly polarized components of equal strength. The direction of their transition dipoles can be in any direction within the plane of the ring, but they are always mutually orthogonal.

The simplest C_2 modulation in the inter-pigment interaction is given by

$$H_2 = V_2 \sum_{n=1}^{N} \cos\left\{2\left[\left(n + \frac{1}{2}\right)\phi - \xi\right]\right\}[|n\rangle\langle n+1| + H.c.]$$

$$+ W_2 \sum_{n=1}^{N} \cos[2(n\phi - \xi)][|n-1\rangle\langle n+1| + H.c.], \quad (4)$$

where V_2 and W_2 are the Fourier amplitudes of wave number 2 of the nearest- and the second-neighbor interactions, respectively. The phase of the modulation is indicated by ξ. Such a perturbation connects exciton states which differ in wave number by 2 or $N - 2$. The matrix element of H_2 between k and $k' = k + 2$ exciton states is (Wu and Small, 1997, 1998)

$$\langle k|H_2|k'\rangle = \exp(2i\xi)\left\{V_2\cos\left(\frac{k+k'}{2}\,\phi\right) + W_2\cos[(k+k')\,\phi]\right\}, \quad (5)$$

and the matrix element between the k and $k' = k + N - 2$ states is

$$\langle k|H_2|k'\rangle = \exp(-2i\xi)\left\{-V_2\cos\left(\frac{k+k'}{2}\,\phi\right) + W_2\cos[(k+k')\,\phi]\right\}. \quad (6)$$

In order to examine the effect of the H_2 perturbation on the exciton states, we assume $W_0/V_0 = W_2/V_2 = 1/8$, because the distance between the second-neighbor pigments is about twice the nearest-neighbor distance. In Fig. 2, the energy levels and the splittings of the degenerate states are plotted as a function of V_2. For the unperturbed ring where $V_2 = 0$, the $k = \pm 1$, ± 2, and ± 3 states are doubly degenerate. As the perturbation sets in, the twofold degeneracy of these states is lifted. The influence of the H_2 perturbation on the lowest exciton states can be understood based on the $\Delta k = 2$ rule for the coupling between the exciton states (see Eq. 5). Because the H_2 perturbation induces interaction between the degenerate $k = \pm 1$ states, the splitting of the $k = \pm 1$ states amounts in first order to $\delta E = 2(V_2 + W_2) = 9V_2/4$. The $k = \pm 2$ states split because one of the two components interacts with $k = 0$, whereas the other does not (see Appendix B). The splitting of the $k = \pm 3$ states is smaller than the $k = \pm 2$ splitting, because the two components interact with the $k = \pm 1$ states and their interaction is weaker than that between the $k = 0$ and one of the $k = \pm 2$ states (see Appendix B). The H_2 perturbation transfers oscillator strength from the optically allowed $k = \pm 1$ states to the $k = \pm 3$ states. However, the absorption intensity of the $k = \pm 1$ and $k = \pm 3$ states can be determined only when the exact orientation of the 18 Q_y transition dipoles is given.

Elliptical deformation of the circular aggregate

In the next step, we want to relate the geometry of the transition moments to the modulation of the interpigment interaction. Since the leading term of the deformation from the circle into an ellipse has the same $\cos(2\theta)$ dependence as the H_2 perturbation, we restrict ourselves to the elliptical deformation in the plane of the ring. In the following sections we will investigate three different arrangements of the 18 pigments on the ellipse. The three models are shown in Fig. 3 as models A, B, and C. In model A the pigments are placed equidistantly on the ellipse. In models B and C the interpigment distance is modulated. The modulation is assumed to have the same symmetry as the ellipse. This means that the modulation reaches its extremes at the principal axes of the ellipse. The interpigment distance is the

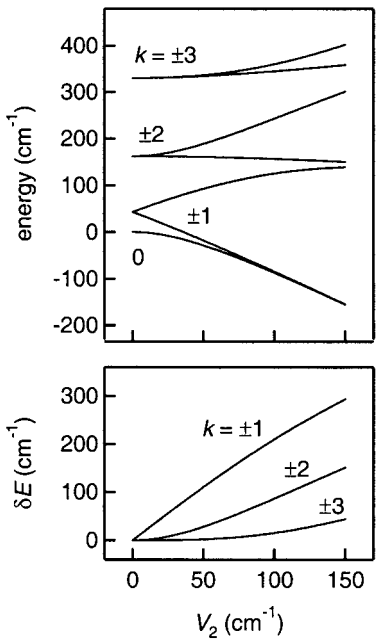

FIGURE 2 Effect of a C_2 perturbation on the exciton manifold of a C_{18} ring aggregate. The energy levels of the $k = 0$, ± 1, ± 2, and ± 3 states and the splitting of the $k = \pm 1$, ± 2, and ± 3 states are plotted as a function of V_2. The nearest-neighbor interaction, V_0, in the unperturbed C_{18} ring is chosen to be -240 cm^{-1}. The second-neighbor interactions, W_0 and W_2, are introduced according to the relation $W_0/V_0 = W_2/V_2 = 1/8$ (see text).

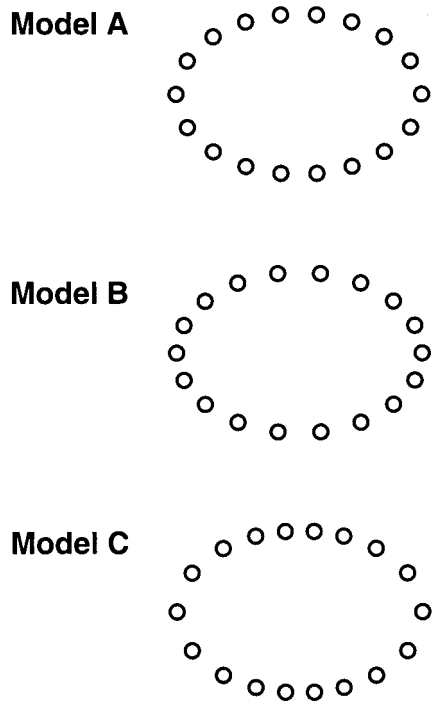

FIGURE 3 Three models for the elliptical deformation. (*A*) Model A; the distance between adjacent molecules is equal over the ring. (*B*) Model B; the distance is shortest at the long axis and longest at the short axis of the ellipse. (*C*) Model C; the distance is longest at the long axis and shortest at the short axis of the ellipse. All the models are drawn for $\delta r/r_0 = 20\%$, i.e., $b/a = (r_0 - \delta r)/(r_0 + \delta r) = 2/3$.

shortest at the long axis and the longest at the short axis of the ellipse in model B and vice versa in model C.

As the simplest approach we take the point-dipole interaction to evaluate the interpigment interaction:

$$V_{nm} \propto \frac{\mu^2}{r_{nm}^3}\kappa_{nm}, \qquad (7)$$

$$\kappa_{nm} = \frac{1}{\mu^2}\left[\vec{\mu}_n \cdot \vec{\mu}_m - 3\frac{(\vec{\mu}_n \cdot \vec{r}_{nm})(\vec{\mu}_m \cdot \vec{r}_{nm})}{r_{nm}^2}\right],$$

where r_{nm} is the distance between the transition dipoles n and m. The orientation factor κ_{nm} is determined by $\vec{\mu}_n$, $\vec{\mu}_m$, and $\vec{r}_{nm}$, the two transition dipoles and the distance vector. In the calculation of an elliptical ring, the interaction is included up to the second neighbors. The absorption of the eigenstates of the elliptical ring is calculated from the wavefunction and the arrangement of the 18 Q_y transition dipoles.

Model A: Equidistant arrangement of the pigments on the ellipse

In this model the pigments are placed equidistantly on an ellipse. When a circular aggregate is deformed into an ellipse, it would be reasonable to reorient the pigments to accommodate the deformation of the ring. This has been taken into account by rotating the Q_y transition moments such that they retain their angle with the local tangent of the ellipse. For a radial deformation of 10% where the long and short axes deviate by 10% from the radius of the circle, i.e., $b/a = (r_0 - \delta r)/(r_0 + \delta r) = 0.9/1.1$, the $k = \pm 1$ splitting is calculated to be only 10 cm^{-1}. Even with a large deformation of $b/a = 1/3$, the splitting is about 50 cm^{-1}, corresponding to $V_2 = 22$ cm^{-1} in Fig. 2. This type of deformation induces little C_2 modulation in the interaction.

The small modulation in the interaction can be understood as follows. Since the interpigment distance is uniform over the ring, the modulation in the nearest-neighbor interaction is entirely due to the orientation of the two transition dipoles and inter-pigment vector (see the orientation factor κ_{nm} in Eq. 7). When the total number of the pigments N is large, the variation of $\vec{\mu}_n \cdot \vec{\mu}_{n+1}$ over the ellipse is small, because the modulation of the dipole angle is divided into N small steps. In the limit of large N the local tangent of the ellipse is represented by the distance vector connecting adjacent pigments $\vec{r}_{n,n+1}$. Since the transition dipoles are oriented in such a way that they retain the angle with the local tangent, the angle between $\vec{\mu}_n$ and $\vec{r}_{n,n+1}$ also stays constant when N is large. As a result, the modulation in the nearest-neighbor interaction is small. Although the cancellation effect is less, the same argument holds for the second-neighbor interaction.

In order to induce a large H_2 perturbation in the equidistant arrangement of Model A, a modulation must be induced that varies the angle between the transition dipole and the local tangent of the ellipse. Such a modulation is introduced by retaining the dipole orientation of the unperturbed circle. The angle between the adjacent transition dipoles is fixed at $\phi = 2\pi/N$. Since the $\vec{r}_{n,n+1}$ vector follows the arc of the deformed ring, this gives rise to the modulation in $\vec{\mu}_n \cdot \vec{r}_{n,n+1}$. The wavefunction of the $k = 0$ state and the two components of the $k = \pm 1$ states are depicted in Fig. 4 for

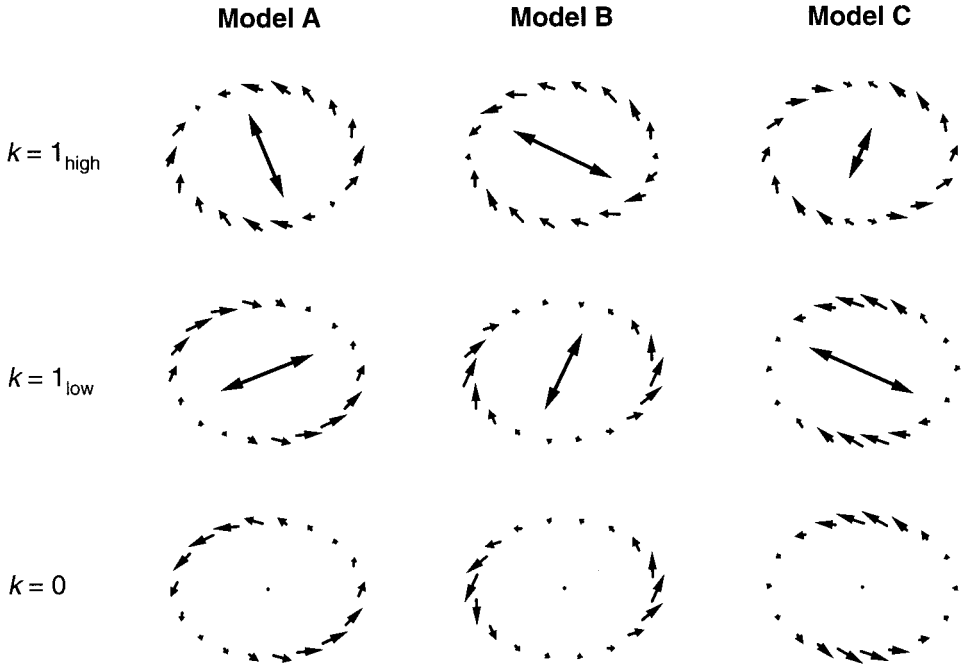

FIGURE 4 Pictorial representation of the $k = 0$, 1_{low}, and 1_{high} states for models A (*left*), B (*middle*), and C (*right*). In Model A, the orientations of the 18 Q_y transition dipoles are fixed at those in the unperturbed C_{18} ring, whereas in models B and C they are adjusted to keep a fixed angle with the local tangent of the ellipse. The arrows indicate the Q_y transition dipoles of the BChl *a* molecules. The length of each arrow is proportional to the amplitude of the exciton wavefunction at the particular pigment position. The bidirectional arrow in the ellipse represents the absorption intensity and its polarization. The ellipse and the wavefunctions are drawn for $\delta r/r_0 = 15\%$.

$\delta r/r_0 = 15\%$, i.e., $b/a = 0.85/1.15$. The lower and the higher components of the $k = \pm 1$ states are denoted by $k = 1_{low}$ and $k = 1_{high}$, respectively. The amplitude of the $k = 0$ wavefunction in Model A is the largest where the dipolar interaction is the strongest, i.e., the two transition dipoles are the most parallel to the direction connecting them. Because the $k = 0$ state has no node, the net transition dipole is zero. The amplitude distribution of the $k = 1_{low}$ state is similar to the $k = 0$ state. However, the $k = 1_{low}$ state has one node. As a result, the state has a finite net transition moment. The bidirectional arrow in Fig. 4 indicates the absorption intensity and its polarization. The $k = 1_{high}$ state also has a finite transition moment. Because the node of the $k = 1_{high}$ state is orthogonal to that of $k = 1_{low}$, the two transition dipoles are mutually orthogonal. However, they do not coincide with the principal axes of the ellipse. The transition dipoles are tilted from the nodes of the wavefunctions and the nodes are tilted from the principal axes of the ellipse.

The energy levels and the splitting of the lowest exciton states for Model A are depicted in the upper two panels of the left column of Fig. 5 as a function of $\delta r/r_0$, the ratio between the radial modulation and the radius of the unperturbed circle. The ratio between the short and the long axes of the ellipse is determined by $\delta r/r_0$ via $b/a = (r_0 - \delta r)/(r_0 + \delta r)$. The overall feature of the figure is similar to Fig. 2, indicating that the deformation predominantly induces the V_2 and W_2 perturbations. The absorption intensities of the $k = \pm 1$ and $k = \pm 3$ states are depicted in the third panel of the left column of Fig. 5. The intensities of $k = 1_{low}$ and 3_{low} states are constant, while the $k = 3_{high}$ state gets oscillator strength from the $k = 1_{high}$ state with increasing perturbation. The angle between the $k = 1_{low}$ and 1_{high} transition dipoles is shown in the lowest panel of the left column of Fig. 5. They are mutually orthogonal within 4 degrees for $\delta r/r_0 < 30\%$.

In summary, the equidistant arrangement of pigments according to Model A yields a small C_2 modulation in interaction if the orientation of the pigments follows the local tangent of the deformed ring. The modulation increases if the orientation of the transition dipoles with respect to the local tangent is modulated.

Models B and C: Modulation of the interpigment distance on the ellipse

In Model B, the inter-pigment distance is assumed to be the shortest at the long axis of the ellipse. An ellipse can be

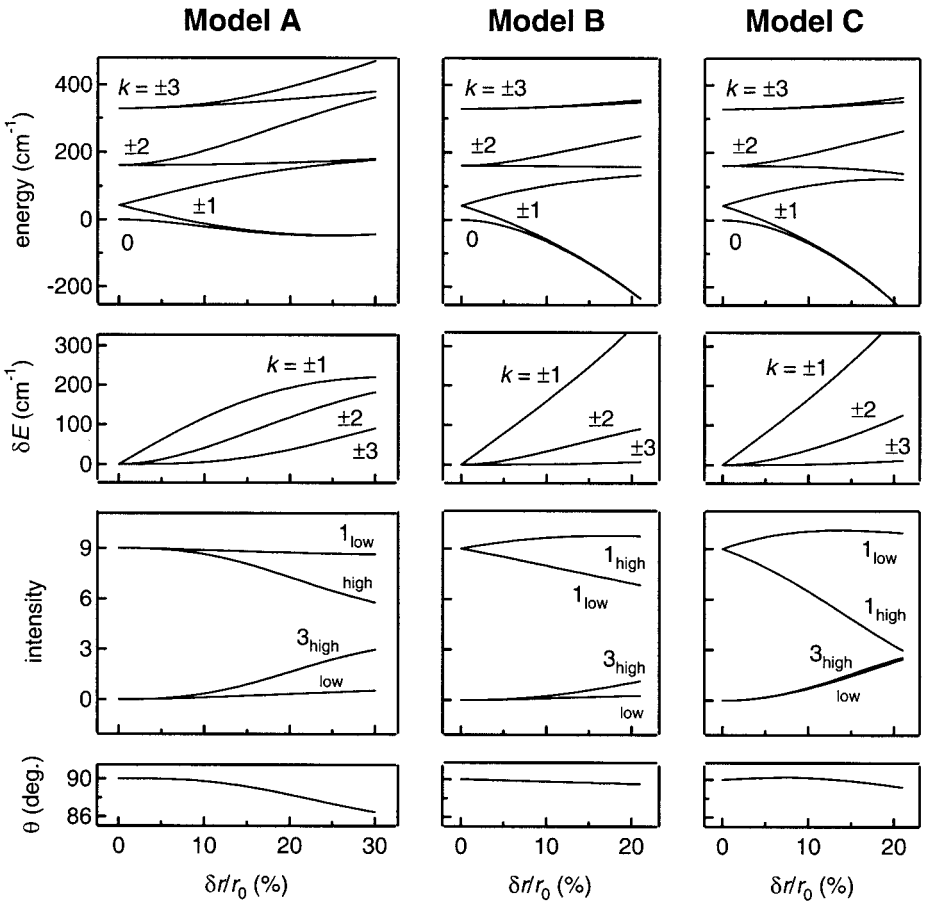

FIGURE 5 Effect of deformation according to models A (*left*), B (*middle*), and C (*right*) on the exciton manifold of a C_{18} ring aggregate. From top to bottom: Energy levels of the $k = 0$, ± 1, ± 2, and ± 3 states. Splitting of the $k = \pm 1$, ± 2, and ± 3 states. Absorption intensity of the $k = 1_{low}$, 1_{high}, 3_{low}, and 3_{high} transitions in units of the monomer absorption. Angle between the two transition dipoles of the $k = 1_{low}$ and 1_{high} states. The nearest-neighbor interaction V_0 in the unperturbed C_{18} ring is chosen to be -240 cm^{-1}.

represented by using a phase parameter χ as $x = a \cos \chi$ and $y = b \sin \chi$. The phase χ of pigment n is fixed at $n\phi$ ($\phi = 2\pi/N$) just like in the unperturbed circle ($a = b$) where the phase χ of pigment n is also $n\phi$. For a given increment $\Delta\chi$ of the phase angle, the interpigment distance is approximated to be the corresponding length Δl of the arc of the ellipse, i.e., $r_{nm} \approx \Delta l \approx \Delta\chi(a^2 \sin^2 \chi + b^2 \cos^2 \chi)^{1/2}$. For a fixed increment of $\Delta\chi = \phi$, the inter-pigment distance at the long axis ($\chi = 0$ or π) is proportional to $dl/d\chi = b$, whereas the distance at the short axis ($\chi = \pm\pi/2$) is proportional to $dl/d\chi = a$. Consequently, the ratio of the interpigment distance at the long axis and at the short axis is b:a.

In Model C, the interpigment distance is assumed to be longest at the long axis of the ellipse. In this model, each pigment is displaced along the line connecting the center of the ring and the position of the pigment in the unperturbed circle. The geometrical angle θ of pigment n measured from the center is fixed at $n\phi$. The inter-pigment distance is approximated to be $r_{nm} \approx \Delta l \approx r(\theta)\Delta\theta$, where $r(\theta)$ is the local radius of the ellipse at the geometrical angle of θ. For a fixed increment of the geometrical angle of $\Delta\theta = \phi$, the interpigment distance is proportional to $r(\theta)$, that is, the distance between the center and the pigment. Therefore, the ratio of the interpigment distance at the long axis and at the short axis is a:b.

The wavefunctions belonging to the $k = 0$ and $k = \pm 1$ states in models B and C are depicted in the middle and the right columns of Fig. 4, respectively. In both models the orientations of the pigments are adjusted to keep a fixed angle with the local tangent of the ellipse. As for Model A, the reorientation of the transition moments minimizes the modulation of the orientation factor κ_{nm}. As a result the variations in the interactions are governed by the modulation of the interpigment distances. The wavefunctions of models B and C are almost identical except for the rotation of 90 degrees with respect to the long and short axes of the ellipse. In both models the amplitude of the wavefunction of the $k = 0$ state is the largest where the interpigment distance is the shortest, resulting from the stronger interaction between the pigments, which yields a decrease of the energy of this state. The $k = 1_{low}$ (1_{high}) state has one node where the interpigment distance is longest (shortest). The extremes of the interpigment distance and the nodes of the wavefunctions coincide with the principal axes of the ellipse. The intensity and polarization of the absorption of the $k = 1_{low}$ and 1_{high} states are shown by the bidirectional arrow in the figure. The transition dipoles of the $k = 1_{low}$ and 1_{high} states are mutually orthogonal, reflecting the orthogonal arrangement of the node of their wavefunctions. However, the transition dipoles do not coincide with the principal axes of the ellipse. They are tilted away from the principal axes by the same amount as the tilt of the individual Q_y transition dipoles from the local tangent.

The energy levels and the splitting of the exciton states as a function of $\delta r/r_0$ are depicted in the upper two panels of the middle and right columns of Fig. 5. The amplitude of V_2 and W_2 can be estimated as follows. For models B and C, the amplitude of the modulation of the interpigment distance $\Delta r_{nm}/r_{nm}$ is $(a - b)/(2r_0) = \delta r/r_0$. Using the $1/r^3$ dependence of the dipolar interaction, the amplitude of the modulation of the interaction will be $V_2/|V_0| \approx W_2/|W_0| \approx 3\Delta r_{nm}/r_{nm} = 3\delta r/r_0$. Thus, the horizontal axis of $\delta r/r_0$ in models B and C in Fig. 5 corresponds linearly to the horizontal axis of V_2 in Fig. 2. Moreover, Fig. 2 and the graphs for models B and C in Fig. 5 show the same effective range for the horizontal axis, since the maximum V_2 of 150 cm^{-1} in Fig. 2 corresponds to the maximum $\delta r/r_0$ of 20% for models B and C in Fig. 5. The first-order splitting of the $k = \pm 1$ states is related to $\delta r/r_0$ by $\delta E = 2(V_2 + W_2) \approx 6|V_0 + W_0|\delta r/r_0$, where the value $V_0 + W_0$ in the unperturbed ring is -270 cm^{-1}.

The intensities of the transitions to the $k = 1_{low}$ and 1_{high} states are different for models B and C in contrast to the splitting and the polarization of these two states (see Fig. 5, third panel, middle and right column). The $k = 1_{high}$ state is stronger than the $k = 1_{low}$ state in Model B and vice versa in Model C. Why is the intensity ratio reversed in the two models? Let us have a closer look at Fig. 4. The wavefunction of the $k = 1_{low}$ state has a larger amplitude around the long axis in Model B and around the short axis in Model C. The amplitude distribution among the major Q_y transition dipole vectors is the same for both models, reflecting the similarity of the wavefunctions. However, these vectors make a larger angle with one another in Model B than in Model C, because the curvature of the ellipse is largest at the long axis and it is smallest at the short axis. Consequently, the sum of the dipole vectors is smaller in Model B than in Model C. The effect of the curvature is more pronounced in the $k = 1_{high}$ state, because the amplitude of the wavefunction of the $k = 1_{high}$ state is distributed more uniformly over the ellipse (see Appendix B). The net transition dipole of the $k = 1_{high}$ state in Model B is much larger than that in Model C.

DISCUSSION

Knowing the spectroscopic properties of the three models, let us compare the models with the experimental observation. A typical fluorescence-excitation spectrum of a single LH2 complex at 1.5 K is depicted in the center of Fig. 6. For comparison, a spectrum taken from a large ensemble is shown on the right-hand side of the figure. The spectrum of the single complex exhibits three absorption peaks, which are obscured in the bulk spectrum. The most important results of a detailed analysis (Ketelaars et al., 2001) of the experimental data for the present work are as follows. 1) The two $k = \pm 1$ states split with an average separation of 110 cm^{-1}. 2) The transition dipoles of the $k = 1_{low}$ and the

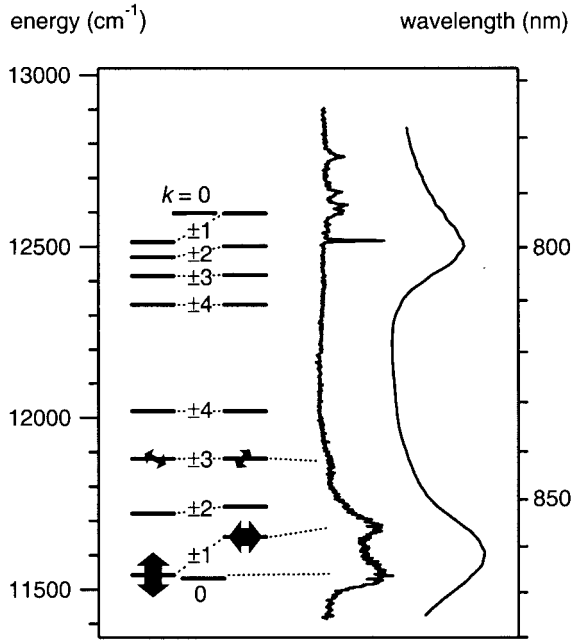

FIGURE 6 The vertical trace in the center of the figure shows the fluorescence-excitation spectrum of a single LH2 complex at 1.5 K. For comparison, the respective spectrum for an ensemble is shown on the right-hand side of the figure. The left part of the figure depicts the energy levels and the transition moments of the exciton states of the B850 ring in C_9 symmetry for an elliptical deformation of $\delta r/r_0 = 7\%$ according to Model C. The parameters used for the unperturbed C_9 ring are $E_\alpha - E_\beta = 240\ cm^{-1}$, $V_i = 254\ cm^{-1}$, $V_e = 226\ cm^{-1}$, $W_\alpha = -35\ cm^{-1}$, and $W_\beta = -25\ cm^{-1}$.

$k = 1_{high}$ states are mutually orthogonal. 3) The intensity of the $k = 1_{high}$ transition is weaker than that of the $k = 1_{low}$ transition, with an average ratio of 0.7. 4) About half of the complexes have an additional weak absorption related to the $k = \pm 3$ states. 5) There is no observable splitting of the $k = \pm 3$ states. 6) The polarization dependence of the $k = \pm 3$ band is weak.

All models described in the present work reproduce the observed $k = \pm 1$ splitting for a deformation of $\delta r/r_0 \approx 10\%$, if the orientation of the pigments is properly chosen. The orthogonality of the two $k = \pm 1$ transitions is maintained in all models within a few degrees. However, the three models differ significantly in their predictions of the intensity ratio between the $k = 1_{low}$ and the $k = 1_{high}$ transitions. In Model A, without reorientation of the pigments, the $k = \pm 1$ splitting of 110 cm^{-1} corresponds to $\delta r/r_0 = 9\%$. For this deformation the intensity ratio of the $k = 1_{high}$ to the $k = 1_{low}$ transitions is 0.98. To reproduce the experimental value of 0.7 for the intensity ratio, a deformation of $\delta r/r_0 = 28\%$ has to be induced, which in turn leads to a separation of the two states of 220 cm^{-1}. Clearly, Model A does not lead to a consistent description of the experimental findings. Model B does not reproduce the observed intensity ratio at all; the $k = 1_{high}$ transition is calculated to be even stronger than the $k = 1_{low}$ transition. Finally, in Model C the observed $k = \pm 1$ splitting of 110 cm^{-1} corresponds to a deformation amplitude of $\delta r/r_0 = 7\%$. This value is in excellent agreement with the value of 8% necessary to explain the observed intensity ratio of 0.7. Thus, only model C explains consistently both the splitting and the intensity ratio of the $k = 1_{low}$ and 1_{high} states.

As yet our analysis has been based on the assumption of C_{18} symmetry for the B850 ring. The question that arises is whether the quantitative agreement between the experimental observations and Model C holds also for the B850 ring in C_9 symmetry. The effect of the deformation according to Model C on the B850 ring in C_9 symmetry is depicted on the left hand side of Fig. 7. The relative interaction strengths for the respective nearest- and second-neighbors were calculated from the crystal structure using the point-dipole approximation. From the simulation of circular dichroism spectra the difference of the excitation energies $E_\alpha - E_\beta$ between the α- and β-bound molecules has been estimated

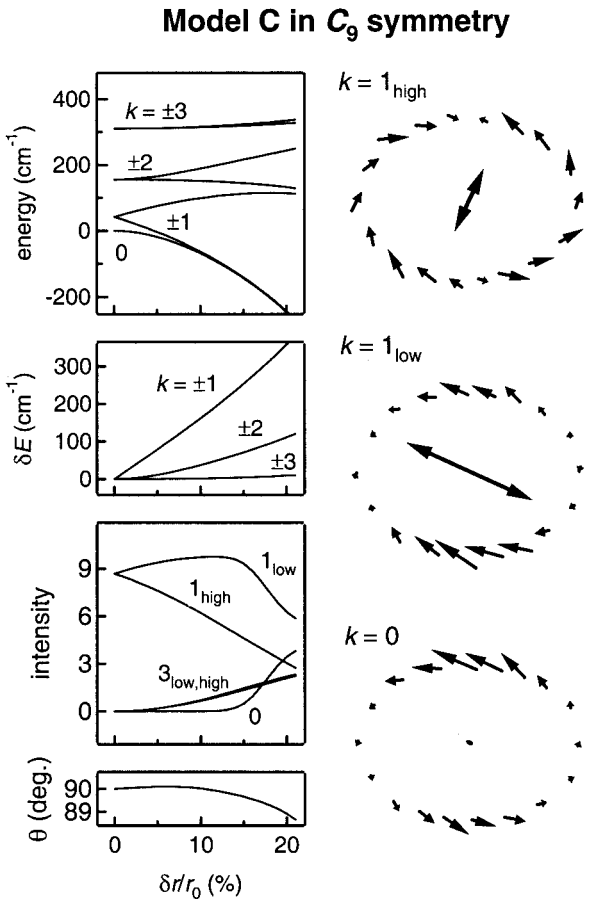

FIGURE 7 Effect of a deformation according to Model C on the B850 ring in C_9 symmetry. *Left*, top to bottom: Energy levels, splittings, absorption intensity of the lowest exciton states, and angle between the $k = 1_{low}$ and 1_{high} transition dipoles. *Right*: Pictorial representation of the wavefunction of the $k = 0$, 1_{low}, and 1_{high} states depicted for $\delta r/r_0 = 15\%$. The parameters used for the unperturbed C_9 ring are the same as those in Fig. 6.

to be about the same as the nearest-neighbor interaction (Scholes and Fleming, 2000; Koolhaas et al., 2000). For the figure it is assumed that $E_\alpha - E_\beta$ is the same as the average nearest-neighbor interaction (240 cm^{-1}). It is seen that the energy levels, splittings, intensity, and the orthogonality are almost the same as those calculated for the C_{18} ring (see the right column of Fig. 5). The only noticeable difference is that a part of the oscillator strength of the $k = 1_{low}$ state is transferred to the $k = 0$ state at large deformations. The mixing between the $k = 1_{low}$ and the $k = 0$ states is caused by the low symmetry of the system. The elliptical ring in the C_{18} approximation has C_2 symmetry. In contrast, the introduction of a C_2 perturbation into the C_9 ring reduces the symmetry of the system to C_1 symmetry. Consequently, the upper half of the deformed ring is no longer equivalent to the lower half of the ring. The same is true for the wavefunctions as shown on the right hand side of Fig. 7 for $\delta r/r_0 = 15\%$. The different amplitude of the upper and lower halves of the $k = 0$ wavefunction produces the non-zero net transition moment.

The left part of Fig. 6 depicts the energy levels and the transition moments of the exciton states calculated for the B850 ring in C_9 symmetry subjected to a deformation of $\delta r/r_0 = 7\%$ according to Model C. The correspondence between the optically allowed exciton states and the observed spectrum is shown by the dotted lines. The relatively narrow spectral features at the top of the exciton manifold around 800 nm originate from the BChl *a* molecules that form the B800 ring, the second circular pigment structure in LH2.

Due to random fluctuations of the protein environment, different pigments within one B850 ring have different excitation energy, which is referred to as intracomplex random disorder. In addition, the average excitation energy differs from one complex to another, which is referred to as intercomplex random disorder (Freiberg et al., 1999; van Oijen et al., 2000; Mostovoy and Knoester, 2000). In the accompanying paper we show that with a proper amount of the intra- and intercomplex disorder, the ensemble absorption spectrum of the B850 band can be reproduced by a Monte Carlo simulation with an elliptical deformation $\delta r/r_0$ of about 7% as described by Model C (Ketelaars et al., 2001). Thus, the Model C elliptical ring of $\delta r/r_0 \approx 7\%$ is consistent with both the individual and the ensemble spectra of LH2.

In the experimental spectra of individual complexes, some of them do not show the $k = \pm 3$ band, whereas others have the $k = \pm 3$ band as strong as the $k = \pm 1$ bands. The large intensity fluctuation of the $k = \pm 3$ band is hard to explain by random disorder, if the deformation is fixed to $\delta r/r_0 = 7\%$. Probably there is a distribution in the deformation, i.e., the ellipticity may differ from one complex to another. The effect of the deformation amplitude $\delta r/r_0$ on the absorption intensity of the $k = 3_{low}$ and 3_{high} states is depicted in the third row of Fig. 5. In models A and B, only the $k = 3_{high}$ state gains oscillator strength as $\delta r/r_0$ increases. Because only one state contributes to the absorption, the polarization dependence of the $k = \pm 3$ band will be strong. In Model C, both components gain oscillator strength equally with increasing $\delta r/r_0$. Since the $k = 3_{low}$ and 3_{high} transitions are mutually orthogonal, the polarization dependence in Model C is weak, in good agreement with the observation. In addition, the splitting of the $k = \pm 3$ states in Model C is less than 10 cm^{-1} for $\delta r/r_0 < 20\%$, which agrees also with the observation that a splitting of these states is not resolved in any complex.

CONCLUSIONS

With the simplest point-dipole approximation for the transition dipole interaction, we have studied the effect of an elliptical deformation on the exciton states of the B850 ring of LH2. An elliptical ring of $b/a \approx 0.9/1.1$ can reproduce the splitting of the $k = \pm 1$ states, while the mutual orthogonality of the absorption of the two components is maintained. However, the intensity ratio between the two $k = \pm 1$ components depends strongly on the arrangement of the pigments on the ellipse. The observed intensity ratio is compatible with a model in which the inter-pigment distance is shortest at the short axis of the ellipse. The observation that the $k = 1_{low}$ absorption is stronger than the $k = 1_{high}$ absorption indicates that the pigments are closer to one other where the curvature of the ellipse is small. This model is also consistent with the weak polarization dependence of the $k = \pm 3$ absorption band. Thus, we have shown that a simple deformation model providing one free parameter of $\delta r/r_0$ can explain the major features of the spectra of individual LH2 complexes.

APPENDIX A

The B850 ring of C_9 symmetry versus the C_{18} approximation

In order to take the difference between the α- and β-bound BChl *a* molecules into account, the Hamiltonian for the B850 ring in C_9 symmetry reads

$$\begin{aligned} H = {} & E_\alpha \sum_{n=1}^{9} |n;\alpha\rangle\langle n;\alpha| + E_\beta \sum_{n=1}^{9} |n;\beta\rangle\langle n;\beta| \\ & + V_i \sum_{n=1}^{9} [|n;\alpha\rangle\langle n;\beta| + H.c.] \\ & + V_e \sum_{n=1}^{9} [|n;\beta\rangle\langle n+1;\alpha| + H.c.] \\ & + W_\alpha \sum_{n=1}^{9} [|n;\alpha\rangle\langle n+1;\alpha| + H.c.] \\ & + W_\beta \sum_{n=1}^{9} [|n;\beta\rangle\langle n+1;\beta| + H.c.]. \end{aligned} \tag{A1}$$

E_α and E_β are the excitation energies of the α- and β-bound molecules, respectively. From the simulation of circular dichroism spectra it was proposed that $E_\alpha > E_\beta$ (Koolhaas et al., 1997). V_i and V_e are the intra- and interdimer nearest-neighbor interactions while W_α and W_β are the second-neighbor interactions between α- and β-bound molecules. Commonly, the direction of the Q_y transition dipole is defined as the direction pointing from the N_{III} to the N_I (or from the N_I to the N_{III}) nitrogen atoms of the BChl *a* molecule. Based on this definition, adjacent transition dipoles are nearly anti-parallel, whereas the second neighbor dipoles are nearly parallel. Consequently, the nearest-neighbor interactions are positive and the second-neighbor interactions are negative, i.e., V_i, $V_e > 0$ and W_α, $W_\beta < 0$. The eigenvalues of the Hamiltonian (A1) are given (Cory et al., 1998; Koolhaas et al., 2000) by

$$E_k^{\pm} = \frac{E_\alpha + E_\beta}{2} + (W_\alpha + W_\beta)\cos(k\delta) \pm \sqrt{[(E_\alpha - E_\beta)/2 + (W_\alpha - W_\beta)\cos(k\delta)]^2 + V_i^2 + V_e^2 + 2V_iV_e\cos(k\delta)\}^{1/2}}, \quad \text{(A2)}$$

where $\delta = 2\pi/9$. For $E_\alpha - E_\beta > 2|W_\alpha - W_\beta|$, the eigenfunctions are written as follows.

$$|k; l\rangle = \frac{1}{\sqrt{9}} \sum_{n=1}^{9} [-\exp(-i\Phi_k)\sin\Theta_k|n; \alpha\rangle + \cos\Theta_k|n; \beta\rangle]\exp(ik\delta n), \quad \text{(A3)}$$

$$|k; u\rangle = \frac{1}{\sqrt{9}} \sum_{n=1}^{9} [\cos\Theta_k|n; \alpha\rangle + \exp(i\Phi_k)\sin\Theta_k|n; \beta\rangle]\exp(ik\delta n), \quad \text{(A4)}$$

where $|k; l\rangle$ and $|k; u\rangle$ denote the upper and lower states, respectively, of wave number k. The angular parameters are given by

$$\tan(2\Theta_k) = \frac{V_i + V_e\cos(k\delta)}{|V_i + V_e\cos(k\delta)|} \times \frac{2[V_i^2 + V_e^2 + 2V_iV_e\cos(k\delta)]}{E_\alpha - E_\beta + 2(W_\alpha - W_\beta)\cos(k\delta)}, \quad \text{(A5)}$$

$$\tan\Phi_k = \frac{V_e\sin(k\delta)}{V_i + V_e\cos(k\delta)}. \quad \text{(A6)}$$

The energy levels of the B850 ring in C_9 symmetry are shown on the left hand side of Fig. 8. The interactions have been calculated from the crystal structure using the point-dipole approximation. The difference of the excitation energies, $E_\alpha - E_\beta$, is assumed to be equal to the average nearest-neighbor interaction (240 cm^{-1}). For comparison, the energy levels of the C_{18} ring are shown on the right-hand side of the figure, assuming average values for the interactions and the excitation energies. The assumption $E_\alpha = E_\beta$ causes the gap between the lower and upper branches of the C_9 ring to become smaller in the C_{18} ring. It is seen that the lower part of the manifold ($k = 0$, ±1, ±2, and ±3) is nearly unaffected by the C_{18} approximation. The effect of this approximation is much smaller than that of the elliptical deformation.

If the α- and β-bound molecules would be equivalent, the expressions for the energy and the wavefunction should correspond to those for the C_{18} ring (Eqs. 2 and 3). Putting $E_0 = E_\alpha = E_\beta$, $V_0 = V_i = V_e$, and $W_0 = W_\alpha = W_\beta$, the energies and the wavefunctions become

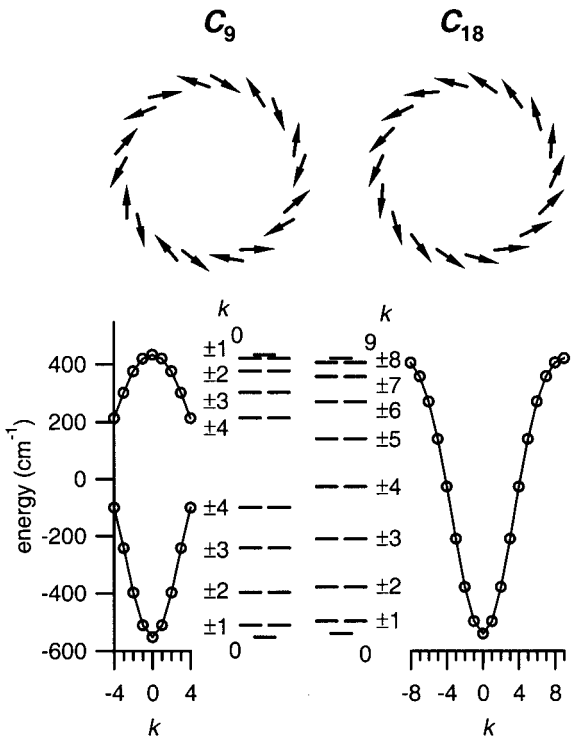

FIGURE 8 *Top*: Physical arrangement of the transition dipoles for C_9 symmetry (*left*) and C_{18} symmetry (*right*). *Bottom*: Exciton manifold of the B850 ring in C_9 symmetry (*left*) and C_{18} symmetry (*right*). The parameters used to describe the C_9 ring are $V_i = 254$ cm^{-1}, $V_e = 226$ cm^{-1}, $W_\alpha = -35$ cm^{-1}, $W_\beta = -25$ cm^{-1}, and $E_\alpha - E_\beta = 240$ cm^{-1}. The parameters used in the C_{18} approximation are $V_0 = -240$ cm^{-1} and $W_0 = -30$ cm^{-1}. The energy is plotted relative to the average excitation energy, $E_0 = (E_\alpha + E_\beta)/2$.

$$E_k^{\pm} = E_0 + 2W_0\cos(k\delta) \pm 2|V_0|\cos(k\delta/2), \quad \text{(A7)}$$

$$|k; l\rangle = \frac{1}{\sqrt{18}} \sum_{n=1}^{9} [-\exp(-ik\delta/2)|n; \alpha\rangle + |n; \beta\rangle]\exp(ik\delta n), \quad \text{(A8)}$$

$$|k; u\rangle = \frac{1}{\sqrt{18}} \sum_{n=1}^{9} [|n; \alpha\rangle + \exp(ik\delta/2)|n; \beta\rangle]\exp(ik\delta n). \quad \text{(A9)}$$

To compare these with Eqs. 2 and 3, the correspondence between the wave numbers k in the two representations has to be made. By reducing the repeating unit from a dimer to a monomer, the first Brillouin zone doubles its width. In the C_{18} ring the wave number runs from -8 to 9, instead of from -4 to 4 as it does in the C_9 ring. The k number of the upper branch in the C_9 ring corresponds to either $-9 - k$ or $9 - k$ in the C_{18} ring (see Fig. 8). Noticing that $\delta = 2\phi$, it is readily seen that the energy expression of Eq. A7 corresponds to Eq. 3.

To compare the wavefunctions, care must be taken for the sign of the nearest-neighbor interaction and the definition of the direction of the transition dipoles. In the C_9 ring α- and β-bound dipoles are defined to be anti-parallel, which means V_i and V_e are positive. In the C_{18} ring, the

symmetry requires that adjacent dipoles are pointing towards the same direction, which means V_0 is negative. Therefore, the wavefunctions appear different, although they represent the same physical arrangement of the transition dipoles. As an example, let us take the lowest state. Starting from the C_9 description, the wavefunction is given by

$$|k = 0; l\rangle = \frac{1}{\sqrt{18}} \sum_{n=1}^{9} [-|n; \alpha\rangle + |n; \beta\rangle]. \quad \text{(A10)}$$

The signs in front of the local function are opposite because the transition dipoles are defined to be anti-parallel. Physically, the adjacent dipoles are pointing into the same direction. The dipole arrangement is identical with that of the $k = 0$ state in the C_{18} ring, which is

$$|k = 0\rangle = \frac{1}{\sqrt{18}} \sum_{n=1}^{18} |n\rangle. \quad \text{(A11)}$$

APPENDIX B

Effect of the C_2 perturbation on the exciton states of a $N = 18$ ring

We will calculate the wavefunction of a $N = 18$ ring aggregate subjected to a C_2 perturbation given by H_2 (see Eq. 4). To make use of the symmetry of the perturbation, we take the following wavefunctions as the basis functions for the doubly degenerate states of $k = \pm 1, \pm 2, \ldots, \pm 8$.

$$|c; k\rangle = \frac{1}{\sqrt{2}} [|+k\rangle e^{-ik\xi} + |-k\rangle e^{ik\xi}]$$

$$= \sqrt{\frac{2}{N}} \sum_n \cos[k(n\phi - \xi)]|n\rangle, \quad \text{(B1)}$$

$$|s; k\rangle = \frac{1}{i\sqrt{2}} [|+k\rangle e^{-ik\xi} - |-k\rangle e^{ik\xi}]$$

$$= \sqrt{\frac{2}{N}} \sum_n \sin[k(n\phi - \xi)]|n\rangle, \quad \text{(B2)}$$

where $k = 1, 2, 3, \ldots, 8$ and $\phi = 2\pi/18$. They are real trigonometric functions having the same phase factor ξ as the H_2 perturbation (see Eq. 4). The lowest nondegenerate $k = 0$ state is a cosine state.

$$|c; 0\rangle = \frac{1}{\sqrt{N}} \sum_n \cos[0(n\phi - \xi)]|n\rangle = \frac{1}{\sqrt{N}} \sum_n |n\rangle. \quad \text{(B3)}$$

Because of the presence of the phase factor ξ the highest nondegenerate $k = 9$ state, $|9\rangle = \Sigma_n (-1)^n |n\rangle/\sqrt{18}$, cannot be expressed by either a cosine or a sine state.

The selection rule of $\Delta k = 2$ or $\Delta k = N - 2$ for the coupling between the k states (Eqs. 5 and 6) is translated into the rules for the trigonometric basis functions as follows: i) The H_2 perturbation has non-zero diagonal elements in the $|c; 1\rangle$, $|s; 1\rangle$, $|c; 8\rangle$, and $|s; 8\rangle$ states. ii) The off-diagonal matrix elements of H_2 are nonzero only between a pair of cosine or sine states which fulfill $\Delta k = 2$. iii) The exceptions to this second rule are the non-zero matrix elements of $\langle c; 8|H_2|s; 8\rangle$, $\langle c; 7|H_2|9\rangle$, and $\langle s; 7|H_2|9\rangle$. As a result of rule i), the first-order energy shift of the degenerate $k = \pm 1$ states is represented in the diagonals of H_2:

$$\langle c; 1|H_2|c; 1\rangle = V_2 + W_2, \quad \text{(B4)}$$

$$\langle s; 1|H_2|s; 1\rangle = -V_2 - W_2. \quad \text{(B5)}$$

The non-zero off-diagonal matrix elements between different k states (except for $k = 9$) are

$$\langle c; 0|H_2|c; 2\rangle = \sqrt{2}[V_2 \cos\phi + W_2 \cos(2\phi)], \quad \text{(B6)}$$

and

$$\langle c; k-1|H_2|c; k+1\rangle = V_2 \cos(k\phi) + W_2 \cos(2k\phi), \quad \text{(B7)}$$

$$\langle s; k-1|H_2|s; k+1\rangle = V_2 \cos(k\phi) + W_2 \cos(2k\phi), \quad \text{(B8)}$$

where $k = 2, 3, \ldots, 7$. Note that the matrix elements listed above are independent of the phase factor ξ of the C_2 modulation. The lowest k states that are relevant for the absorption spectrum are not sensitive to the phase factor ξ. The remaining non-zero matrix elements between the highest k states depend on the phase factor ξ:

$$\langle c; 8|H_2|c; 8\rangle = (-V_2 + W_2)\cos(18\xi), \quad \text{(B9)}$$

$$\langle s; 8|H_2|s; 8\rangle = (V_2 - W_2)\cos(18\xi), \quad \text{(B10)}$$

$$\langle c; 8|H_2|s; 8\rangle = (V_2 - W_2)\sin(18\xi), \quad \text{(B11)}$$

$$\langle c; 7|H_2|9\rangle = \sqrt{2}[-V_2 \cos\phi + W_2 \cos(2\phi)]\cos(9\xi), \quad \text{(B12)}$$

$$\langle s; 7|H_2|9\rangle = \sqrt{2}[V_2 \cos\phi - W_2 \cos(2\phi)]\sin(9\xi). \quad \text{(B13)}$$

Two of the three off-diagonal matrix elements become zero at $\xi = 0$ and $\pi/18$. At these phase angles, the interaction is more symmetric than C_2 because the position of the maximum of the H_2 modulation (Eq. 4) coincides with one of the pigments at $\xi = 0$ or it bisects two pigments at $\xi = \pi/18$. As a consequence the $k = 9$ state is described as a cosine (sine) state at $\xi = 0$ ($\pi/18$), i.e., $|9\rangle = |c; 9\rangle = \Sigma_n \cos[9(n\phi - 0)]|n\rangle/\sqrt{18}$ ($\xi = 0$) and $|9\rangle = -|s; 9\rangle = -\Sigma_n \sin[9(n\phi - \pi/18)]|n\rangle/\sqrt{18}$ ($\xi = \pi/18$). Vanishing of the matrix elements accords with the general rule that cosine states do not interact with sine states, i.e., $\langle s; 7|H_2|c; 9\rangle = 0$ ($\xi = 0$), $\langle c; 7|H_2|s; 9\rangle = 0$ ($\xi = \pi/18$), and $\langle c; 8|H_2|s; 8\rangle = 0$ ($\xi = 0, \pi/18$).

The lowest exciton manifold in Fig. 2 is calculated based on the matrix elements given by Eqs. B4 through B13. The manifold is plotted against a single parameter of V_2 by assuming $W_0/V_0 = W_2/V_2 = 1/8$. The nearest-neighbor interaction, V_0, is fixed at $-240\ \text{cm}^{-1}$. The eigenfunctions of the $k = 0$, 1_{low}, and 1_{high} states at $V_2 = 110\ \text{cm}^{-1}$ are given by

$$|0\rangle = 0.85|c; 0\rangle - 0.53|c; 2\rangle, \quad \text{(B14)}$$

$$|1_{low}\rangle = 0.98|s; 1\rangle - 0.20|s; 3\rangle, \quad \text{(B15)}$$

$$|1_{high}\rangle = 0.92|c; 1\rangle - 0.40|c; 3\rangle. \quad \text{(B16)}$$

The mixing with one state separated by $\Delta k = 2$ is sufficient to describe these lowest three states. Contamination with other, higher states is less than 0.2% for all the three states. The wavefunctions belonging to these three states are shown in Fig. 9. Because $V_2/|V_0|$ is set to $110/|240| \approx 45\%$, the wavefunctions in Fig. 9 correspond to the wavefunctions in Fig. 4 depicted for models B and C at $\delta r/r_0 = 15\%$. Note that $V_2/|V_0| = 3\delta r/r_0$ in models B and C. The mixing in the $|0\rangle$ state is the largest, reflecting the strongest interaction between the $|c; 0\rangle$ and $|c; 2\rangle$ states (see Eq. B6). The interaction between the $|c; 1\rangle$ and $|c; 3\rangle$ states is the same as that between the $|s; 1\rangle$ and $|s; 3\rangle$ states (see Eqs. B7 and B8). However, the mixing of the states is larger in the $k = 1_{high}$ state than in the $k = 1_{low}$ state, because the first-order energy difference between the $|c; 1\rangle$ and $|c; 3\rangle$ states is smaller

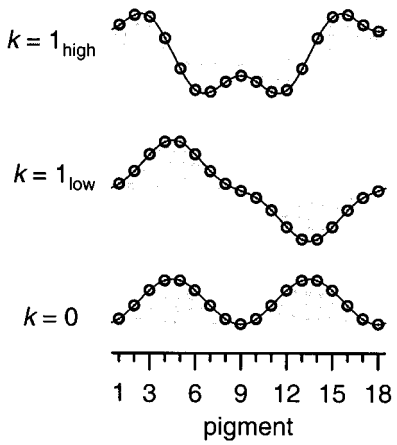

FIGURE 9 Wavefunctions belonging to the $k = 0$, 1_{low}, and 1_{high} states of a C_{18} ring aggregate subjected to a C_2 perturbation. The nearest-neighbor interactions used for the calculation are $V_0 = -240$ cm^{-1} and $V_2 = 110$ cm^{-1}. The second-neighbor interactions, W_2 and W_0, are introduced according to the relation $W_2/V_2 = W_0/V_0 = 1/8$. These wavefunctions correspond to the wavefunctions in Fig. 4 depicted for models B and C (see text).

(see Eqs. B4 and B5). As a consequence, the amplitude of the wavefunction of the $k = 1_{high}$ state is more uniformly distributed over the entire ellipse than in the $k = 1_{low}$ state.

We thank Prof. J. P. Abrahams, Prof. J. Knoester, and Prof. J. H. van der Waals for helpful discussions. This work is part of the research program of the Stichting voor Fundamenteel Onderzoek der Materie (FOM) with financial aid from the Nederlandse Organisatie voor Wetenschappelijk Onderzoek (NWO) and is also supported by the Section Earth and Life Sciences (ALW) of the Netherlands Organization for Scientific Research (NWO) and by the Volkswagen-Stiftung (Hannover, Germany).

REFERENCES

Alden, R. G., E. Johnson, V. Nagarajan, W. W. Parson, C. J. Law, and R. G. Cogdell. 1997. Calculations of spectroscopic properties of the LH2 bacteriochlorophyll-protein antenna complex from *Rhodopseudomonas acidophila*. *J. Phys. Chem. B.* 101:4667–4680.

Bopp, M. A., Y. Jia, L. Li, R. J. Cogdell, and R. M. Hochstrasser. 1997. Fluorescence and photobleaching dynamics of single light-harvesting complexes. *Proc. Natl. Acad. Sci. USA.* 94:10630–10635.

Bopp, M. A., A. Sytnik, T. D. Howard, R. J. Cogdell, and R. M. Hochstrasser. 1999. The dynamics of structural deformations of immobilized single light-harvesting complexes. *Proc. Natl. Acad. Sci. USA.* 96: 11271–11276.

Cory, M. G., M. C. Zerner, X. Hu, and K. Schulten. 1998. Electronic excitations in aggregates of bacteriochlorophylls. *J. Phys. Chem. B.* 102:7640–7650.

Freiberg, A., K. Timpmann, R. Ruus, and N. W. Woodbury. 1999. Disordered exciton analysis of linear and nonlinear absorption spectra of antenna bacteriochlorophyll aggregates: LH2-only mutant chromatophores of *Rhodobacter sphaeroides* at 8 K under spectrally selective excitation. *J. Phys. Chem. B.* 103:10032–10041.

Ketelaars, M., A. M. van Oijen, M. Matsushita, J. Köhler, J. Schmidt, and T. J. Aartsma. 2001. Spectroscopy on the B850 band of individual light-harvesting 2 complexes of *Rhodopseudomonas acidophila*; I. Experiments and Monte Carlo simulations. *Biophys. J.* 80:1591–1603.

Koolhaas, M. H. C., G. van der Zwan, R. N. Frese, and R. van Grondelle. 1997. Red shift of the zero crossing in the CD spectra of the LH2 antenna complex of *Rhodopseudomonas acidophila*: a structure-based study. *J. Phys. Chem. B.* 101:7262–7270.

Koolhaas, M. H. C., R. N. Frese, G. J. S. Fowler, T. S. Bibby, S. Georgakopoulou, G. van der Zwan, C. N. Hunter, and R. van Grondelle. 1998. Identification of the upper exciton component of the B850 bacteriochlorophylls of the LH2 antenna complex, using a B800-free mutant of *Rhodobacter sphaeroides*. *Biochemistry.* 37:4693–4698.

Koolhaas, M. H. C., G. van der Zwan, and R. van Grondelle. 2000. Local and nonlocal contributions to the linear spectroscopy of light-harvesting antenna systems. *J. Phys. Chem. B.* 104:4489–4502.

Krueger, B. P., G. D. Scholes, and G. R. Fleming. 1998. Calculation of couplings and energy-transfer pathways between the pigments of LH2 by the ab initio transition density cube method. *J. Phys. Chem. B.* 102:5378–5386.

McDermott, G., S. M. Prince, A. A. Freer, A. M. Hawthornthwaite-Lawless, M. Z. Papiz, R. J. Cogdell, and N. W. Isaacs. 1995. Crystal structure of an integral membrane light-harvesting complex from photosynthetic bacteria. *Nature.* 374:517–521.

Mostovoy, M. V., and J. Knoester. 2000. Statistics of optical spectra from single ring-aggregates and its application to LH2. *J. Phys. Chem. B.* 104:12355–12364.

Sauer, K., R. J. Cogdell, S. M. Prince, A. Freer, N. W. Isaacs, and H. Scheer. 1996. Structure-based calculations of the optical spectra of the LH2 bacteriochlorophyll-protein complex from *Rhodopseudomonas acidophila*. *Photochem. Photobiol.* 64:564–576.

Scholes, G. D., I. R. Gould, R. J. Cogdell, and G. R. Fleming. 1999. *Ab initio* molecular orbital calculations of electronic couplings in the LH2 bacterial light-harvesting complex of *Rps. Acidophila*. *J. Phys. Chem. B.* 103:2543–2553.

Scholes, G. D., and G. R. Fleming. 2000. On the mechanism of light harvesting in photosynthetic purple bacteria: B800 to B850 energy transfer. *J. Phys. Chem. B.* 104:1854–1868.

Sundström, V., T. Pullerits, and R. van Grondelle. 1999. Photosynthetic light-harvesting: reconciling dynamics and structure of purple bacterial LH2 reveals function of photosynthetic unit. *J. Phys. Chem. B.* 103: 2327–2346.

Tietz, C., O. Chekhlov, A. Dräbenstedt, J. Schuster, and J. Wrachtrup. 1999. Spectroscopy on single light-harvesting complexes at low temperature. *J. Phys. Chem. B.* 103:6328–6333.

van Oijen, A. M., M. Ketelaars, J. Köhler, T. J. Aartsma, and J. Schmidt. 1998. Spectroscopy of single light-harvesting complexes from purple photosynthetic bacteria at 1.2 K. *J. Phys. Chem. B.* 102:9363–9366.

van Oijen, A. M., M. Ketelaars, J. Köhler, T. J. Aartsma, and J. Schmidt. 1999a. Spectroscopy of individual LH2 complexes of *Rhodopseudomonas acidophila*: localized excitations in the B800 band. *Chem. Phys.* 247:53–60.

van Oijen, A. M., M. Ketelaars, J. Köhler, T. J. Aartsma, and J. Schmidt. 1999b. Unraveling the electronic structure of individual photosynthetic pigment-protein complexes. *Science.* 285:400–402.

van Oijen, A. M., M. Ketelaars, J. Köhler, T. J. Aartsma, and J. Schmidt. 2000. Spectroscopy of individual light-harvesting 2 complexes of *Rhodopseudomonas acidophila*: diagonal disorder, intercomplex heterogeneity, spectral diffusion, and energy transfer in the B800 band. *Biophys. J.* 78:1570–1577.

Wu, H.-M., and G. J. Small. 1997. Symmetry adapted basis defect patterns for analysis of the effects of energy disorder on cyclic arrays of coupled chromophores. *Chem. Phys.* 218:225–234.

Wu, H.-M., and G. J. Small. 1998. Symmetry-based analysis of the effects of random energy disorder on the excitonic level structure of cyclic arrays: application to photosynthetic antenna complexes. *J. Phys. Chem. B.* 102:888–898.